Left-right asymmetry of the hippocampal synapses with differential subunit allocation of glutamate receptors

Yoshiaki Shinohara[a,b,1], Hajime Hirase[b], Masahiko Watanabe[c], Makoto Itakura[d], Masami Takahashi[d], and Ryuichi Shigemoto[a,e]

[a]Division of Cerebral Structure, National Institute for Physiological Sciences, Okazaki 444-8787, Japan; [b]Hirase Research Unit, RIKEN Brain Science Institute, Wako 351-0198, Japan; [c]Department of Anatomy, Hokkaido University, Sapporo 060-8638, Japan; [d]Department of Biochemistry, Kitasato University School of Medicine, Sagamihara 228-8555, Japan; and [e]Solution Oriented Research for Science and Technology, Japan Science and Technology Agency, Kawaguchi 332-0012, Japan

Edited by Richard L. Huganir, Johns Hopkins University School of Medicine, Baltimore, MD, and approved October 16, 2008
(received for review July 31, 2008)

Left-right asymmetry of the brain has been studied mostly through psychological examination and functional imaging in primates, leaving its molecular and synaptic aspects largely unaddressed. Here, we show that hippocampal CA1 pyramidal cell synapses differ in size, shape, and glutamate receptor expression depending on the laterality of presynaptic origin. CA1 synapses receiving neuronal input from the right CA3 pyramidal cells are larger and have more perforated PSD and a GluR1 expression level twice as high as those receiving input from the left CA3. The synaptic density of GluR1 increases as the size of a synapse increases, whereas that of NR2B decreases because of the relatively constant NR2B expression in CA1 regardless of synapse size. Densities of other major glutamate receptor subunits show no correlation with synapse size, thus resulting in higher net expression in synapses having right input. Our study demonstrates universal left-right asymmetry of hippocampal synapses with a fundamental relationship between synaptic area and the expression of glutamate receptor subunits.

hippocampus | laterality | NMDA receptor | AMPA receptor | spine

Although lateral specializations of the brain, such as lingual specialization in the left cerebral hemisphere, have been of great interest for years (1), the molecular and structural basis for functional brain asymmetry has remained largely elusive (2). One of the reasons that hinder molecular and anatomical dissection of brain lateralization at the synaptic level is a difficulty observing brain asymmetry in mice, the most molecularly tractable mammalian model system. In our previous study, we found asymmetrical distributions of NR2B subunits of NMDA receptors in the mouse hippocampus (3). Ipsilateral CA3-CA1 pyramidal cell synapses in the stratum radiatum (SR) in the left CA1 were 1.5 times more sensitive to NR2B subunit specific antagonist than those in the right CA1. The contralateral CA3-CA1 pyramidal synapses had the opposite asymmetry (Fig. 1*A*).

Among ionotropic glutamate receptor subunits, six major glutamate receptor subunits (GluR1, GluR2, GluR3, NR1, NR2A, and NR2B) are expressed in the hippocampal CA1 pyramidal cell synapses (4). Rearrangement of these receptor subunit compositions serves as a molecular switch for synaptic plasticity (5). Induction of synaptic plasticity in many brain regions requires NMDA receptor activation, and although the exact molecular mechanism is not fully understood, the ratio of NR2A/NR2B subunit plays a role in determining the direction of synaptic plasticity (6, 7). When synaptic activity is elevated upon the induction of long-term potentiation (LTP), GluR1-containing AMPA receptors are inserted into postsynaptic sites (8). Such synaptic insertion of GluR1 is necessary for an enlargement of spines (9, 10), which accompanies LTP induction.

In this study, we investigated left-right asymmetry of mouse hippocampal synapses at the molecular and structural levels. We found that the synaptic sizes differed between CA1 pyramidal cell synapses receiving input from the left and the right CA3 pyramidal cells. In addition, we observed unique correlations between synapse size and the expression of different glutamate receptor subunits.

Results

Hippocampal CA1 pyramidal neurons receive major excitatory inputs from ipsilateral (ie, Schaffer) and contralateral (ie, commissural) fibers originating from CA3 pyramidal neurons (Fig. 1*A*). To examine the morphological characteristics of CA1 synapses formed with CA3 pyramidal neurons in the right and left hemispheres, we injected vesicular stomatitis virus glycoprotein-G-coated lentivirus expressing green fluorescent protein (GFP) into the left or right CA3 pyramidal cell layer (Fig. 1*B*; $n = 3$ each). After injection, GFP-filled axons were apparent in the ipsi- and contralateral CA1 (Fig. 1*B*). Because vesicular stomatitis virus glycoprotein-G-coated lentivirus serves exclusively for anterograde tracing (11), no CA3 pyramidal neurons were labeled in the contralateral side of the injection. By using electron microscopy, we examined CA1 apical dendrite spines in synaptic contact with labeled axon terminals in serial ultrathin sections (Fig. 1*C*).

Postsynaptic density (PSD) area and spine head volume were measured from spines making contact ipsilaterally (L $\rightarrow$ L, $n = 118$; R $\rightarrow$ R, $n = 121$) and contralaterally (L $\rightarrow$ R, $n = 135$; R $\rightarrow$ L, $n = 123$) with CA3 projecting axons. Surprisingly, significant differences were detected in both spine head volume and PSD area between all combinations of synapses receiving CA3 projections from the opposite sides (Fig. 1*D*; Mann-Whitney test, $P < 0.005$ for L $\rightarrow$ L vs. R $\rightarrow$ L; $P < 0.001$ for other combinations). However, no significant difference was detected between synapses receiving ipsilateral and contralateral projections originating from the same side. The average PSD area in the CA1 SR spines making contact with axons originating in right

Author contributions: Y.S. designed research; Y.S. performed research; M.W., M.I., and M.T. contributed new reagents/analytic tools; Y.S. analyzed data; and Y.S., H.H., and R.S. wrote the paper.

The authors declare no conflict of interest.

This article is a PNAS Direct Submission.

Freely available online through the PNAS open access option.

[1]To whom correspondence should be addressed. E-mail: shinohara@brain.riken.jp.

This article contains supporting information online at www.pnas.org/cgi/content/full/0807461105/DCSupplemental.

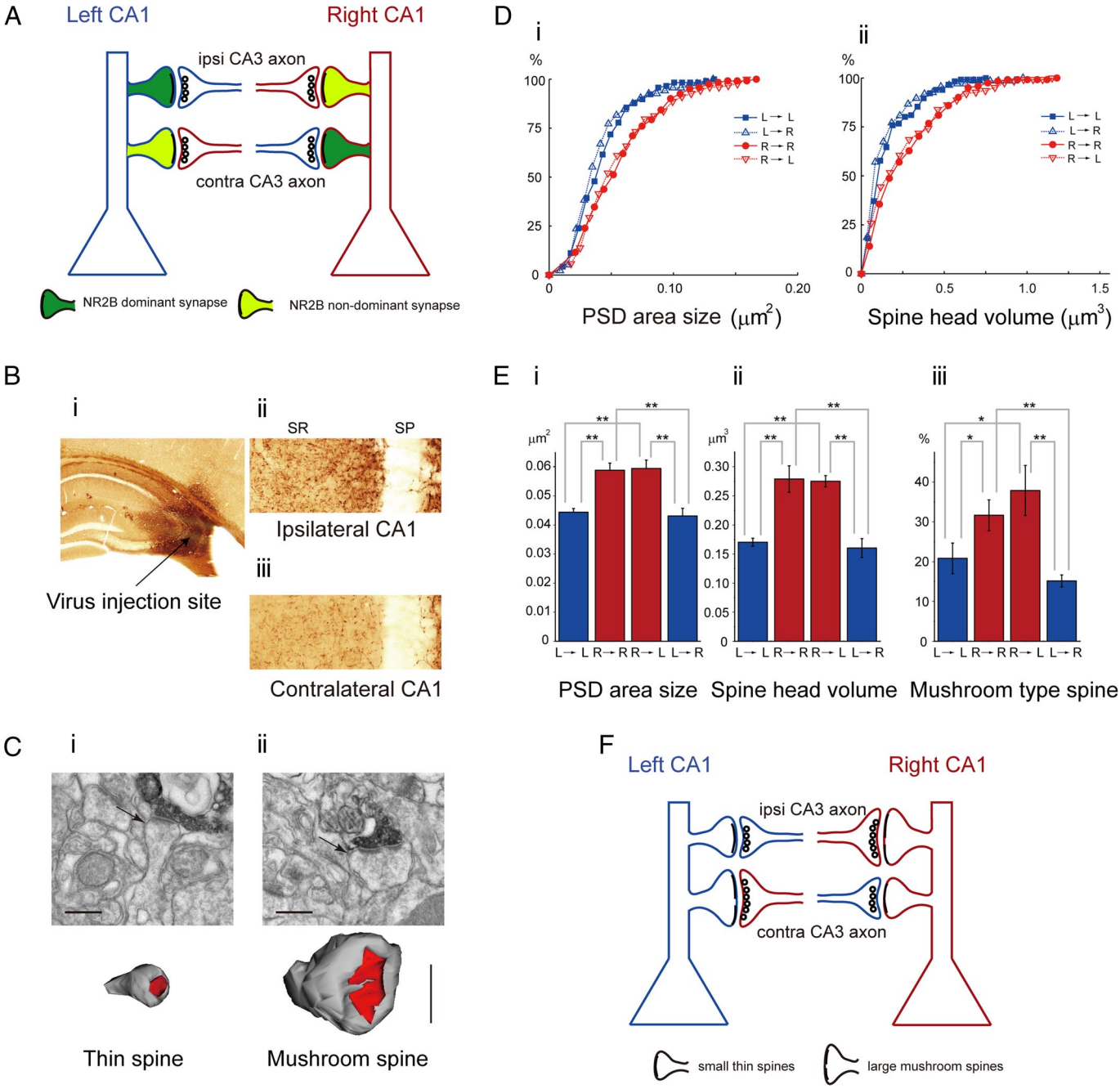

Fig. 1. Morphology of CA1 pyramidal cell apical dendrite spines and synapses is dependent on the laterality of presynaptic CA3 pyramidal cell. (*A*) Schematic illustration of left (blue) and right (red) CA1 pyramidal cells having NR2B dominant (dark green) and NR2B non-dominant (light green) synapses. The diagram was derived from Kawakami *et al* (3). (*B*) GFP-expressing lentivirus was injected unilaterally into the CA3 pyramidal cell layer (arrow in *i*). Axons and their terminals were heavily labeled for GFP in ipsilateral (*ii*) and contralateral (*iii*) CA1 SR. SP, *stratum pyramidale*. (*C*) GFP-labeled axon terminals were clearly observed by electron microscopy (*Upper*), and the spines making synapses (arrows) with labeled terminals were reconstructed using serial ultrathin sections (*Lower*). Reconstructed spines were classified as thin (*i*) or mushroom-type (*ii*) spines. Mushroom spines are defined as those with perforated PSDs (in red). (Scale bars, 300 nm.) (*D*) Cumulative percentile distributions of PSD area size (*i*) and spine head volume (*ii*). Those parameters were measured for the spines making synapses with ipsilateral (L → L, blue filled square, R → R, red filled circle) and contralateral (L → R, blue open triangle, R → L, red open triangle) projections in CA1. L, left; R, right. (*E*) Average PSD area (*i*), spine head volume (*ii*), and percentage of mushroom-type spines (*iii*) were calculated from three animals. Blue and red bars indicate left and right presynaptic origins, respectively. Statistically significant differences were detected between all combinations of red and blue bar data (mean ± SD; *, $P < 0.05$; **, $P < 0.01$). Error bars represent SD. (*F*) Asymmetrical morphology of CA1 pyramidal cell synapses. Left CA3-originated axons (blue) make synapses more frequently with small thin CA1 spines, whereas right CA3-originated axons (red) make synapses more frequently with large mushroom-type CA1 spines.

CA3 pyramidal neurons was ≈40% larger than that in the spines with axons originating in left CA3 pyramidal neurons (Fig. 1*E*; 0.0590 μm^2 vs. 0.0435 μm^2; $P < 0.001$). The head volume of the CA1 spines in contact with right CA3 pyramidal neurons was also 70% greater (Fig. 1*E*; 0.278 μm^3 vs. 0.166 μm^3; $P < 0.001$) than the head volume of the spines contacting left CA3 pyramidal neurons. Approximately 35% of the spines forming synapses with right CA3 pyramidal neurons had "mushroom-type"

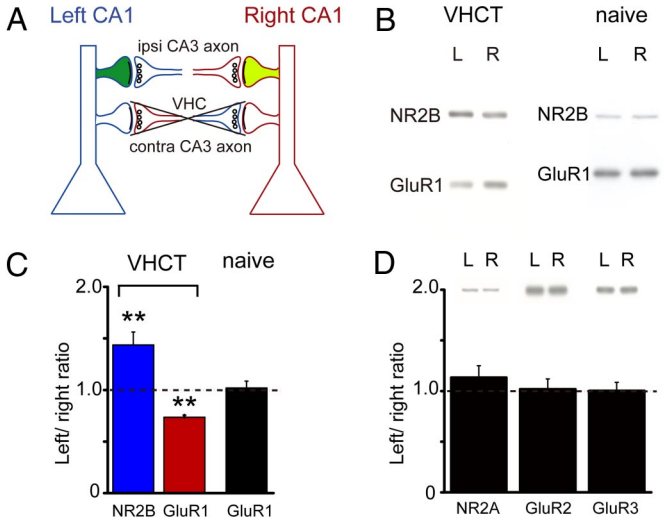

Fig. 2. Asymmetrical expression of NR2B and GluR1 subunits in hippocampal synapses. (*A*) Conceptual diagram of VHC transected (VHCT) mice model, in which CA3 axons projecting to contralateral CA1 degenerate. The coloring scheme is the same as that in Fig. 1*A*. (*B*) Western blot analysis of NR2B and GluR1 subunits in PSD fractions prepared from the left and the right CA1 SR of VHCT or naïve mice. In VHCT mice, NR2B immunoreactivity was higher in the left than in the right, whereas that of GluR1 was higher in the right. The data were obtained from the same acrylamide gels. No asymmetry of GluR1 immunoreactivity was detected in naïve mice. (*C*) Left/right ratios of NR2B and GluR1 immuno-reactivities were measured in PSD fractions prepared from CA1 SR ($n = 3$). Ratios of optical densities (left/right) in VHCT mice significantly deviated from 1.0 and from those for GluR1 observed in naïve mice ($n = 3$ for each;**, $P < 0.01$, *t* test). Error bars represent SD. (*D*) No asymmetry of subunit expression was detected for NR2A, GluR2, and GluR3 in VHCT mice ($n = 3$).

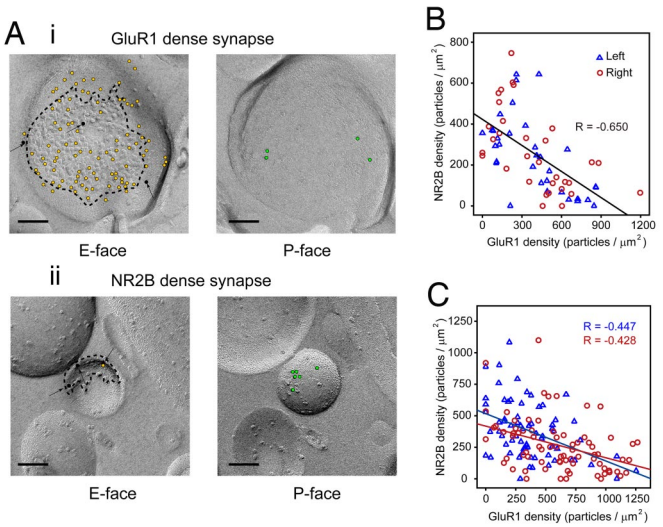

Fig. 3. Inverse correlation between NR2B and GluR1 densities in individual synapses. (*A*) Paired SDS-FRL from GluR1-dense (*i*) and NR2B-dense (*ii*) synapses in VHCT mice. Immuno-gold particles for GluR1 (in yellow) and NR1 (in black and arrows) were observed in E-face, and for NR2B (in green) were in P-face. (Scale bars, 100 nm.) (*B*) Inverse correlation between NR2B and GluR1 labeling densities in individual synapses in a naïve mouse. Synapses in the left and right sides are plotted in blue and red, respectively. (*C*) Labeling densities for NR2B and GluR1 subunits in VHCT mice. Data from two VHCT mice were pooled. Each mouse showed a significant inverse correlation between GluR1 and NR2B labeling ($R_s = -0.597$, $P < 0.01$; $R_s = -0.438$, $P < 0.01$).

morphology and perforated PSDs (12). In contrast, less than 20% of the spines making contact with left CA3 pyramidal neurons were classified as mushroom-type (Fig. 1 *C* and *E*). Two-way ANOVA revealed that the laterality of presynaptic CA3 neurons had a strong correlation with PSD size and spine head volume ($F = 35.1$, $P < 0.0001$ for PSD area; $F = 38.6$, $P < 0.0001$ for spine head volume), whereas the laterality of postsynaptic CA1 neurons did not ($F = 0.17$, $P = 0.682$ for PSD area; $F = 0.06$, $P = 0.806$ for spine head volume). These results indicate that CA1 spine morphology is determined by the laterality of presynaptic CA3 neurons rather than by the laterality of postsynaptic CA1 neurons (Fig. 1*F*).

We then compared the synaptic expression of major ionotropic glutamate receptor subunits by immunoblotting PSD fractions prepared from the CA1 SR of ventral hippocampal commissure transected (VHCT) mice (Fig. 2*A*). In VHCT mice, CA1 pyramidal cells would have exclusively ipsilateral projections from CA3 5 days after surgery (3, 13), as the VHC conveyed commissural fibers. Because the great majority of glutamatergic synapses in the SR is found on pyramidal cell spines, contamination from synapses on interneurons is virtually negligible. Interestingly, immunoreactivity for GluR1 was 40% higher in the right PSD fraction than in the left ($n = 3$; $P < 0.01$; 22, 26, and 18 mice were used in each trial) whereas immunoreactivity for NR2B was 40% higher in the left than in the right (Fig. 2 *B* and *C*) as previously reported (3). No asymmetry of GluR1 protein expression was detected in naïve (ie, un-operated) mice (Fig. 2 *B* and *C*). In VHCT mice, no significant asymmetrical expressions were found for other major subunits of glutamate receptors (Fig. 2*D*, for NR1 see ref. 3). These results led to a hypothesis that the "NR2B non-dominant synapses" in CA1 pyramidal cells (Fig. 1*A*, light green) are likely to be "GluR1-dominant synapses."

We questioned whether the reciprocal expression pattern of GluR1 and NR2B was reflected at the level of individual synapses. To label synaptic surface receptors, we used the SDS freeze-fracture replica labeling (SDS-FRL) method (14) with double replica [supporting information (SI) Fig. S1]. This method allows us to quantitatively detect two different molecules without interference from steric hindrance (14). An excitatory synaptic area is distinguished by the clustering of intramembrane particles (IMPs) on the E-face (14) and positive labeling for NR1 NMDA receptor subunit (Fig. 3*A*). In the CA1 SR, immuno-gold labelings for GluR1 on the E-face and NR2B on the P-face were concentrated in excitatory postsynaptic areas marked by IMP clusters (Fig. 3*A* and Fig. S2). Within those synaptic areas, NR2B-rich and GluR1-rich domains were mildly segregated (Fig. S3). Because fracture of the cell membrane and exposure of a synaptic area are random and often partial, we measured the labelings density (i.e., the number of gold particles per exposed synaptic area) in individual synapses. In naïve animals, the average labeling densities for GluR1 (left, 395 particles/μm^2; right, 402 particles/μm^2) and NR2B (left, 246 particles/μm^2; right, 267 particles/μm^2) were not significantly different (Mann-Whitney test) between the left and the right CA1 SR. In VHCT animals, the average labeling densities for GluR1 (left, 370 particles/μm^2; right, 608 particles/μm^2) and NR2B (left, 378 particles/μm^2; right, 265 particles/μm^2) differed significantly between the left and right hemispheres (Mann-Whitney test, $P < 0.001$ for GluR1 and $P < 0.005$ for NR2B), consistent with the immunoblot results from PSD fractions (Fig. 2 *B* and *C*). In the naïve mouse, the densities of NR2B and GluR1 labeling displayed a clear inverse correlation (Fig. 3*B*; Spearman correlation coefficient [R_s] $= -0.651$, $n = 33$ for left; $R_s = -0.660$, $n = 33$ for right; $R_s = -0.650$, combined; $P < 0.01$ for each case). A similar inverse correlation between NR2B and GluR1 labeling densities was also observed in VHCT mice (Fig. 3*C*; $R_s = -0.447$, $n = 70$ for left; $R_s = -0.428$, $n = 76$ for right; $R_s = -0.493$, combined; $P < 0.01$ for each case).

NR2A subunits have been proposed to replace NR2B subunits during development or as a consequence of synaptic strengthening (15). We therefore investigated a possible correlation between the synaptic densities of NR2A and NR2B (Figs. S3 and S4); however, we did not detect any significant correlation between the labeling densities for NR2A and NR2B subunits in VHCT mice (Fig. S4; $R_s = 0.202$, $n = 63$ for left; $R_s = -0.035$, $n = 64$ for right; $R_s = 0.096$, combined). No significant left-right asymmetry in NR2A labeling was detected, thus confirming the data in Fig. 2*D*, whereas a significant left-right difference in NR2B density was detected in the same pair of replicas ($P < 0.005$). In addition, there was no significant correlation between GluR1 and NR2A densities (data not shown).

Because the synapses receiving input from the right side were relatively large and rich in GluR1 and those receiving input from the left side were smaller and rich in NR2B, we investigated if levels of GluR1 and NR2B would show any correlation with the size of a synapse. To directly investigate the relationship between synapse size and synaptic levels of GluR1 and NR2B, we performed post-embedding immuno-gold labeling for GluR1 or NR2B using serial ultrathin sections from naïve mice. Dense labeling for GluR1 was found mostly at large synapses, whereas dense NR2B labeling was frequently associated with small synapses (Fig. 4*A*). The number of GluR1 immuno-gold particles in reconstructed individual synapses showed a strong positive correlation with the synaptic area (Pearson correlation coefficient [R_p] = 0.785, $P < 0.01$, $n = 93$), whereas the number of NR2B immuno-gold particles did not ($R_p = 0.161$, no significance, $n = 102$; Fig. 4*B*). These results suggest that the total amount of NR2B per synapse is relatively constant regardless of the synapse size. The labeling density of each subunit was subsequently calculated by dividing the gold particle number by the total synaptic area. There was a weak, yet significant, positive correlation between the synaptic area and labeling density for GluR1 ($R_p = 0.423$, $P < 0.01$), implying that the expression level of GluR1 subunit per synapse has a supra-linear relationship to PSD area size (Fig. 4*C*). Conversely, a hyperbolic fit ($y = 3.385/x$, $F = 170.8$) rather than the linear regression ($F = 16.4$) better explained the relationship between NR2B labeling density and synapse size (Fig. 4*C*). This negative correlation is consistent with the higher density of NR2B in the left CA1 of VHCT mice (Fig. 2 *B* and *C* and Fig. 3*C*). For NR1 and NR2A, we found no correlation between IMP cluster size and their labeling densities, showing that the levels of these subunits in individual synapses are proportional to the synapse size (Fig. S5; also see Fig. S3).

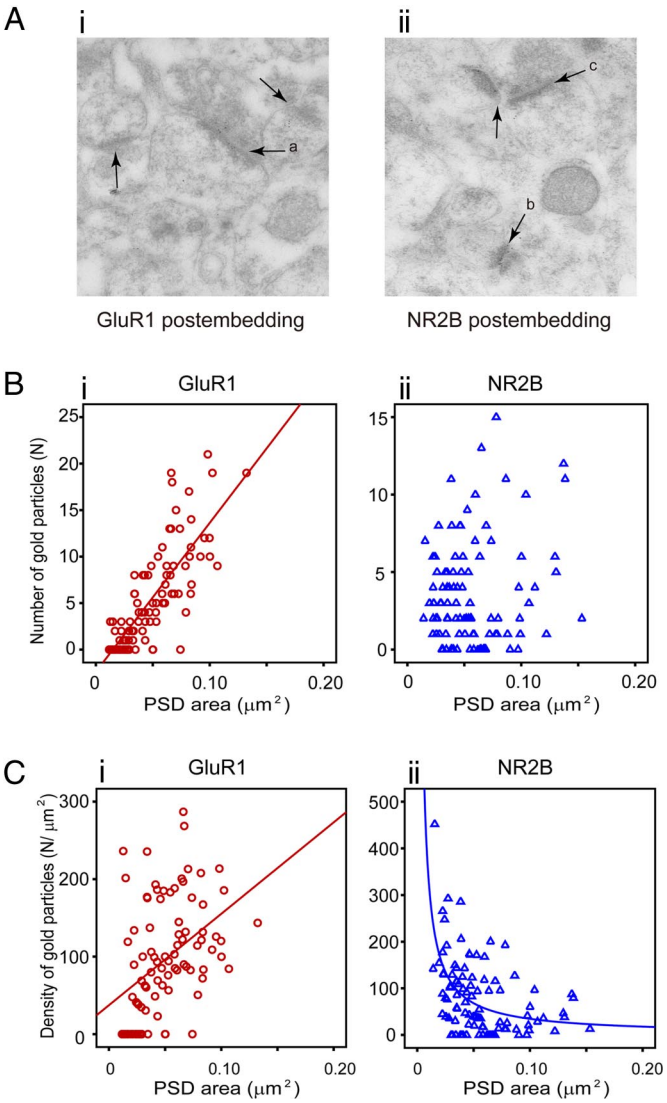

Fig. 4. Relationship between expression of synaptic GluR1/NR2B subunits and postsynaptic area as revealed by the post-embedding method. (*A*) Electron micrographs displaying post-embedding immuno-gold labeling for GluR1 (*i*) and NR2B (*ii*) in spine synapses (arrows) in CA1 SR. Note that gold particles for GluR1 are abundant in the large spine (*a*), whereas NR2B gold particles are more concentrated in the small spine (*b*) compared with the large spine (*c*). (*B*) Relationship between the number of gold particles for synaptic GluR1 (*i*, red) or NR2B (*ii*, blue) and postsynaptic area. The total area of each synapse was measured from serial sections. Data from two VHCT mice were pooled. (*C*) Relationship between the density of synaptic GluR1 (*i*, red) or NR2B (*ii*, blue) labeling and postsynaptic area. A significant positive correlation was seen between GluR1 density and postsynaptic area, whereas a hyperbolic (i.e., 1/x) fit described the relation well for NR2B.

Discussion

This report identifies morphological left-right asymmetry at the synaptic level. We found that the size of a synapse had a significant correlation with the laterality of the presynaptic innervation in the apical dendrite of hippocampal CA1 pyramidal cells (Fig. 5*A*). In addition, individual expression patterns of ionotropic glutamate receptor subunits exhibited a close relation to the size of a synapse. We therefore propose a simple principle (Fig. 5*B*) in which asymmetrical distributions of glutamate receptors in CA1 pyramidal cells can be explained by the relationship between sizes of glutamatergic synapses and the levels of ionotropic glutamate receptor subunits in individual synapses.

Postsynaptic Properties of CA1 Pyramidal Cell Synapses Are Determined by Laterality of Presynaptic CA3 Neurons. One of our main findings in the current study is that the size and receptor allocation of CA1 pyramidal cell synapses are determined by the laterality of presynaptic axon arising from CA3 pyramidal cells (Fig. 5*A*). When outputs from the CA3 are conveyed to CA1, the information derived from the left and the right CA3 is processed differently through NR2B dense and GluR1 dense synapses, respectively. Although it is unclear if this kind of input-dependent asymmetry observed in mice might have any relation to the well known functional lateralization of the hippocampus in primates, it is worth noting that the monkey, as well as the human, has few commissural projections from the CA3 area (16). If the left and right inputs into the primate hippocampus are also asymmetrically processed in CA1 pyramidal cells, it should result in asymmetrical hippocampal outputs through the lateralized activity in CA1. Further investigation of left-right asymmetry in primates is thus required to elucidate the relevance of the present results to the functional lateralization of the brain.

Because synaptic efficacy is closely associated with neural activities, the formation of the input-dependent asymmetry seen in our

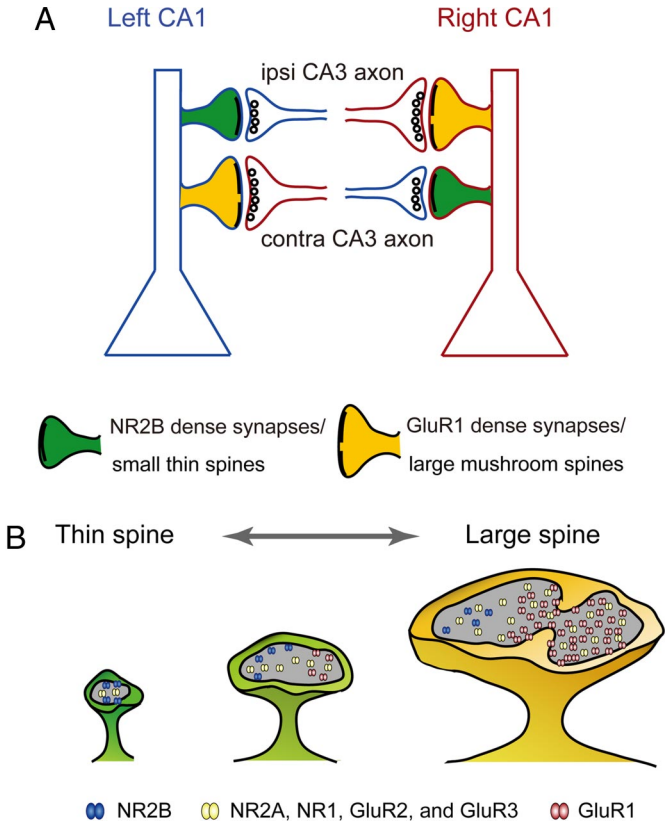

Fig. 5. Left-right asymmetry of hippocampal synapses with differential distributions of glutamate receptors. (*A*) Asymmetry of CA1 pyramidal cell synapses. Both left (blue) and right (red) CA1 pyramidal cells frequently make NR2B dense, small synapses on thin spines (green) with axon terminals from left CA3 pyramidal cells (blue) and GluR1 dense, large synapses on mushroom-type spines (yellow) with axon terminals from the right (red). (*B*) Relationship between glutamate receptor density and synaptic area. NR2B (blue) density is negatively correlated to the synapse area, resulting in relatively constant receptor expression regardless of synaptic size. GluR1 (red) density increases as a synapse becomes larger (shown in green to yellow). Expression of other subunits (yellow) is proportional to the synaptic area.

study might have been a result of differential neural activities in the left and the right CA3. However, because of the dense commissural projections of CA3 pyramidal cells in mice, an activity level on one side may not be sufficiently distinct to generate asymmetry among the levels of postsynaptic receptors. Alternatively, the asymmetry may be genetically programmed. It is possible that axon terminals originating from the left and the right CA3 express different molecular cues during the formation of CA3-CA1 projections in development. We recently discovered the lack of hippocampal left-right asymmetry in *iv* mutant mice (17), in which the left-right asymmetry is affected by a spontaneous genetic mutation in an axonemal dynein (18). This strongly supports that the left-right asymmetry of the murine hippocampus is subject to a genetically controlled program. In the downstream of *iv*, certain guidance molecules required for the formation of the commissural projections during development (19) may also be involved in the establishment of the left-right asymmetry.

Inverse Correlation Between GluR1 and NR2B Synaptic Densities. We observed a positive correlation between the synaptic GluR1 density and synaptic area, whereas the NR2B density was negatively correlated. Although synaptic mechanisms governing receptor subunit stoichiometry have been extensively investigated, most of the studies were conducted *in vitro*. Our study found a clear relationship between the densities of two glutamatergic receptor subunits *in vivo*. Recently, specific roles of GluR1 subunit in LTP have been identified *in vitro*, and LTP apparently causes rapid enlargement of spines and recruitment of GluR1 into dendritic spines (9, 10). This suggests that the relatively large spine head volume observed in our study may have been caused by LTP. More recently, an *in vivo* study demonstrated that newly synthesized GluR1 subunits were specifically transported into mushroom-type spines in the hippocampus after fear conditioning (20). Although GluR1-containing AMPA receptors have been reported to be rapidly replaced by GluR2-containing receptors *in vitro* (21), in our study we observed constant abundance of GluR1 expression in large spines. It is therefore conceivable that the *in vivo* mechanism of chronic synaptic plasticity differs to some extent from that of acutely induced synaptic plasticity *in vitro*.

Although NMDA receptor subunit compositions and their importance in synaptic plasticity have attracted considerable attention, molecular evidence that directly links subunit composition changes to altered levels of synaptic AMPA receptors is relatively scarce. Consistent with previous *in vitro* studies (22), we often encountered a segregated localization of GluR1 and NR2B within the same synapse when a large IMP cluster was present (Fig. S3), suggesting that higher NR2B subunit density can suppress synaptic expression of GluR1 subunits. This is in high contrast with uniform AMPA and NMDA distributions in the spinal dorsal horn (23), and may imply the presence in the hippocampus of unique synaptic scaffold proteins associated with these receptors (24, 25). In addition to the guidance molecules discussed earlier, investigation of left-right asymmetry in PSD protein expression is necessary for a better understanding of asymmetrical receptor allocation.

Although the reciprocal relationship between NR2B and GluR1 might be expected as discussed earlier, we detected no such relationship between NR2B and NR2A. NR2A replaces NR2B-containing NMDA receptors upon ligand stimulation (15) or during development. Moreover, an *in vitro* study has shown that the activation of NR2A-containing NMDA receptors is required for surface insertion of GluR1-containing AMPA receptors (22). It might be reasonable to anticipate the presence of reversal asymmetry of NR2A as seen in GluR1. However, in accordance with the hypothesis that the NR2A/NR2B ratio is a determinant of the direction of synaptic plasticity (6, 7), our results suggest that higher NR2A/NR2B ratio, but not higher NR2A density, may be sufficient to induce the higher expression of GluR1-containing AMPA receptors.

Receptor Density Diversity in Relation to Synapse Size and Asymmetrical Expression. Based on the relationship between receptor density and synapse area observed in this study, we propose that spines and their glutamate receptor subunits can be classified into three groups (Fig. 5*B*). The first group consists of glutamate receptor subunits whose level is relatively constant regardless of the size of a synapse, thus yielding a hyperbolic negative correlation line between the receptor density and the synapse size. Note that NR2B belongs to this group. Because there is no significant difference in the total number of synapses or in the number of Schaffer collateral synapses between the left and right CA1 areas (13) (Fig. S6), net expression of NR2B is actually symmetrical between the left and right hemispheres, as well as between the GluR1 dense synapses and the NR2B dense synapses. The second group consists of the subunits having a constant receptor density regardless of the synapse size. NR1, NR2A, GluR2, and GluR3 belong to this group. These receptor subunits are expressed at higher levels in GluR1 dense synapses than those in NR2B dense synapses because the former is, in general, larger than the latter. This results in asymmetrical net expression of the receptors. In the third group, the density of

each receptor subunit increases with the synapse size, and GluR1 was found to belong to this group. The level of receptor expression increases supra-linearly with the synapse size. The level of GluR1 in GluR1 dense synapses was more than twice the level found in NR2B dense synapses (i.e., 1.6 times [increase in density (from SDS-FRL)] $\times$ 1.4 times [increase in synaptic size]), resulting in an enhanced left-right asymmetry. These three distinct patterns of receptor density-synapse area relationship are thus reflected in the differential left-right asymmetry in net expression of glutamate receptor subunits in the hippocampus.

Methods

For labeling of Shaffer and commissural axon terminals, a GFP-expressing lentivirus was pinpoint-injected unilaterally into the CA3 area (Fig. S7), and 3 weeks later, GFP was immunostained. Observation of CA1 spine morphology was performed by electron microscopy of serial sections. VHC transection and immunoblotting of PSD fractions were performed as previously described (3). SR of the left and right CA1 area was trimmed and used for biochemical purification of the PSD fraction. For SDS-FRL, fixed tissues were first frozen by a high-pressure freezing machine and replicated with carbon and platinum (14). After SDS treatment, the replicas were immuno-labeled with antibodies for GluR1 (Fig. S8), NR1, NR2A, and NR2B. For post-embedding immuno-labeling, fixed tissue was frozen and embedded into hydrophobic resin (HM20). Serial ultrathin sections were subjected to immuno-labeling. For detailed materials and methods, see *SI Text*.

ACKNOWLEDGMENTS. We are grateful to S. Yamada, H. Maebashi, and S. Hara for technical support; P. Osten and Y. Fukazawa for GFP-expressing lentivirus; S. Mitani for GFP antibody; R. Sprengel for GluR1-knockout mice; J. Fiala for Reconstruct software; S. Nakanishi for densitometer; and J. Kitano, K. Imoto, Y. Miyashita, and M. Kengaku for helpful comments. This work was supported by Ministry of Education, Culture, Sports, Science, and Technology of Japan grants 19300114 and 18700344 and the Japan Society for Promotion of Science. H.H. acknowledges support from Human Frontier Science Program (HFPS) RGY0073/2006-C.

1. Toga AW, Thompson PM (2003) Mapping brain asymmetry. *Nat Rev Neurosci* 4:37–48.
2. Sun T, Walsh CA (2006) Molecular approaches to brain asymmetry and handedness. *Nat Rev Neurosci* 7:655–662.
3. Kawakami R, *et al.* (2003) Asymmetrical allocation of NMDA receptor epsilon2 subunits in hippocampal circuitry. *Science* 300:990–994.
4. Wisden W, Seeburg PH (1993) Mammalian ionotropic glutamate receptors. *Curr Opin Neurobiol* 3:291–298.
5. Shi SH, *et al.* (1999) Rapid spine delivery and redistribution of AMPA receptors after synaptic NMDA receptor activation. *Science* 284:1811–1816.
6. Morishita W, *et al.* (2007) Activation of NR2B-containing NMDA receptors is not required for NMDA receptor-dependent long-term depression. *Neuropharmacology* 52:71–76.
7. Yashiro K, Philpot BD (2008) Regulation of NMDA receptor subunit expression and its implications for LTD, LTP, and metaplasticity. *Neuropharmacology* 55:1081–1094.
8. Park M, Penick EC, Edwards JG, Kauer JA, Ehlers MD (2004) Recycling endosomes supply AMPA receptors for LTP. *Science* 305:1972–1975.
9. Park M, *et al.* (2006) Plasticity-induced growth of dendritic spines by exocytic trafficking from recycling endosomes. *Neuron* 52:817–830.
10. Kopec CD, Real E, Kessels HW, Malinow R (2007) GluR1 links structural and functional plasticity at excitatory synapses. *J Neurosci* 27:13706–13718.
11. Grinevich V, Brecht M, Osten P (2005) Monosynaptic pathway from rat vibrissa motor cortex to facial motor neurons revealed by lentivirus-based axonal tracing. *J Neurosci* 25:8250–8258.
12. Popov VI, *et al.* (2004) Remodelling of synaptic morphology but unchanged synaptic density during late phase long-term potentiation (LTP): a serial section electron micrograph study in the dentate gyrus in the anaesthetised rat. *Neuroscience* 128:251–262.
13. Wu Y, *et al.* (2005) Target-cell-specific left-right asymmetry of NMDA receptor content in Schaffer collateral synapses in epsilon1/NR2A knock-out mice. *J Neurosci* 25:9213–9226.
14. Masugi-Tokita M, *et al.* (2007) Number and density of AMPA receptors in individual synapses in the rat cerebellum as revealed by SDS-digested freeze-fracture replica labeling. *J Neurosci* 27:2135–2144.
15. Barria A, Malinow R (2002) Subunit-specific NMDA receptor trafficking to synapses. *Neuron* 35:345–353.
16. Gloor P, Salanova V, Olivier A, Quesney LF (1993) The human dorsal hippocampal commissure. An anatomically identifiable and functional pathway. *Brain* 116(part 5):1249–1273.
17. Kawakami R, Dobi A, Shigemoto R, Ito I (2008) Right isomerism of the brain in inversus viscerum mutant mice. *PLoS ONE* 3:e1945.
18. Supp DM, Witte DP, Potter SS, Brueckner M (1997) Mutation of an axonemal dynein affects left-right asymmetry in inversus viscerum mice. *Nature* 389:963–966.
19. Cheng HJ, *et al.* (2001) Plexin-A3 mediates semaphorin signaling and regulates the development of hippocampal axonal projections. *Neuron* 32:249–263.
20. Matsuo N, Reijmers L, Mayford M (2008) Spine-type-specific recruitment of newly synthesized AMPA receptors with learning. *Science* 319:1104–1107.
21. Shi S, Hayashi Y, Esteban JA, Malinow R (2001) Subunit-specific rules governing AMPA receptor trafficking to synapses in hippocampal pyramidal neurons. *Cell* 105:331–343.
22. Kim MJ, Dunah AW, Wang YT, Sheng M (2005) Differential roles of NR2A- and NR2B-containing NMDA receptors in Ras-ERK signaling and AMPA receptor trafficking. *Neuron* 46:745–760.
23. Antal M, *et al.* (2008) Numbers, densities, and colocalization of AMPA- and NMDA-type glutamate receptors at individual synapses in the superficial spinal dorsal horn of rats. *J. Neurosci* 28:9692–9701.
24. O'Brien RJ, Lau LF, Huganir RL (1998) Molecular mechanisms of glutamate receptor clustering at excitatory synapses. *Curr Opin Neurobiol* 8:364–369.
25. Kim E, Sheng M (2004) PDZ domain proteins of synapses. *Nat Rev Neurosci* 5:771–781.